

Waveguiding inside the complete band gap of a phononic crystal slab

Fu-Li Hsiao

Institut FEMTO-ST, Département LPMO, CNRS UMR 6174, Université de Franche-Comté, 32 avenue de l'Observatoire, 25044 Besançon cedex, France and Department of Optics and Photonics, National Central University, Jung-Li 320, Taiwan

Abdelkrim Khelif, Hanane Moubchir, and Abdelkrim Choujaa

Institut FEMTO-ST, Département LPMO, CNRS UMR 6174, Université de Franche-Comté 32 avenue de l'Observatoire, 25044 Besançon cedex, France

Chii-Chang Chen

Department of Optics and Photonics, National Central University Jung-Li, 320, Taiwan

Vincent Laude

Institut FEMTO-ST, Département LPMO, CNRS UMR 6174, Université de Franche-Comté 32 avenue de l'Observatoire, 25044 Besançon cedex, France

(Received 27 April 2007; published 8 November 2007)

The propagation of acoustic waves in a square-lattice phononic crystal slab consisting of a single layer of spherical steel beads in a solid epoxy matrix is studied experimentally. Waves are excited by an ultrasonic transducer and fully characterized on the slab surface by laser interferometry. A complete band gap is found to extend around 300 kHz, in good agreement with theoretical predictions. The transmission attenuation caused by absorption and band gap effects is obtained as a function of frequency and propagation distance. Well confined acoustic wave propagation inside a line-defect waveguide is further observed experimentally.

DOI: [10.1103/PhysRevE.76.056601](https://doi.org/10.1103/PhysRevE.76.056601)

PACS number(s): 43.20.+g, 43.40.+s, 46.40.Cd, 63.20.-e

I. INTRODUCTION

The propagation of elastic waves in inhomogeneous media has attracted much attention over the last years. Phononic crystals are media with periodically varying elastic coefficients that can exhibit complete acoustic band gaps depending on the composition and the geometry as well as on the nature of the constitutive materials [1,2]. For frequencies within a complete band gap, there can be no vibration and no propagation of acoustic waves, whatever the polarization and the wave vector. In such a situation, a phononic crystal behaves similar to a perfect mirror and can be modified further to gain control over acoustic waves. This principle can be used to obtain acoustic cavities, acoustic filters, or very efficient waveguides by adding certain defects to the lattice [3–9]. All these functions can be achieved in a very tight space of the order of some acoustic wavelengths.

Recently, there has been a growing interest in phononic crystal slabs, whose thickness is finite in the direction perpendicular to the surfaces [10–13]. For simplicity, we refer in the following to this direction as the vertical direction. Wave propagation in phononic crystal slabs requires all vibration directions to be taken into account, resulting in a full three dimensional problem. The slab geometry is naturally well suited for making waveguides where guided modes are strongly confined vertically between the two surfaces. This is especially true for solid slabs in air or a vacuum, as we consider specifically in this work, and in contrast with photonic crystal slabs, in which energy can radiate out of the slab into the surrounding medium [14].

Since slabs can in principle be made as thin as required, it is expected that a two-dimensional periodic structuration will

produce a three-dimensional confinement of waves inside a complete band gap [12]. This effect has, however, not been demonstrated experimentally up to now, to the best of our knowledge. Complete band gaps have been observed previously in solid-solid two-dimensional phononic crystals excited by bulk waves [15]. However, the presence of the two surfaces limiting the slab and the finite thickness strongly influence the band structure. Some recent theoretical studies of phononic crystal slabs have considered cylindrical inclusions in a host material with a strong contrast of acoustic properties [10–12]. It was in particular found that the complete band gaps of phononic crystal slabs can be quite different from those of an equivalent infinite crystal. Experimental studies have been reported for air holes etched in a thin plate [16] and for a thin phononic film on a silicon homogeneous plate [17]. These structures presented band gaps for some propagation directions, but no complete band gap was observed.

The purpose of this paper is to demonstrate experimentally a complete band gap in a phononic crystal slab and to investigate the propagation of acoustic waves within it. The system we have chosen is a finite thickness, solid/solid, and surface free phononic crystal slab. This system lends itself to numerical simulation by a finite element method developed previously [12]. Furthermore, by using a combination of ultrasonic electrical transduction and optical detection by a laser interferometer, we obtain maps of the propagation of waves at any monochromatic frequency. This experimental setup is used to quantify the attenuation on propagation and the confinement of acoustic energy within a line-defect waveguide.

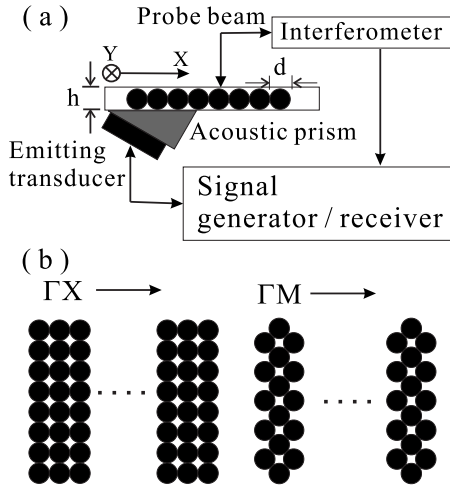


FIG. 1. Sketch of the experiment. (a) Waves are excited in a phononic crystal slab using an ultrasonic transducer through a prism with an incidence angle of 30° . The phononic crystal slab is formed by a one layer thick array of spherical steel beads with a diameter of 4 mm arranged according to a square lattice in an epoxy matrix. (b) Measurements along the ΓX and ΓM directions are required to characterize the phononic crystal properties. The corresponding sample arrangements are depicted.

II. METHODS

The experimental setup is sketched in Fig. 1. The structures used in our experiments are two-dimensional square lattice arrays of spherical steel beads embedded in an epoxy matrix (Epotech E501). The two dimensional square lattice arrays were assembled by placing the beads carefully by hand. The beads are very monodisperse with a diameter of 4 mm, and the thickness of the epoxy plate is also 4 mm. Figure 1(b) illustrates the lattice arrangement of the two samples required to characterize the phononic crystal properties. The lattice constant of the square lattice is 4 mm, i.e., each bead is in contact with four of its neighbors. The mass density and the shear and longitudinal velocities of acoustic waves in steel and epoxy are displayed in Table I. The choice of steel and epoxy as the composite materials was originally based on the strong contrast in their densities and elastic constants, as is generally the case when complete band gaps are sought for. Expressed using the acoustic impedance for longitudinal waves, this contrast is approximately 16.4.

The ultrasonic wave signal incident into the phononic crystals is launched by a wide-bandwidth acoustic transducer (Panametrics immersion transducer type Videocan V301).

TABLE I. Material constants of the phononic crystal constituents. c_S and c_L are the velocities for shear and longitudinal waves, respectively, ρ is the mass density, and Z_L is the acoustic impedance for longitudinal waves.

	c_S (m s $^{-1}$)	c_L (m s $^{-1}$)	ρ (kg m $^{-3}$)	Z_L (MRayles)
Steel	3200	5800	7780	45.124
Epoxy	1100	2500	1100	2.75

An acoustic prism is inserted between the transducer and the phononic crystals slab. The acoustic wave is incident into the slab with an angle of 30° . This angle was chosen experimentally in order to excite efficiently slab modes propagating parallel to the surfaces. The phononic crystal slab, the transducer, and the acoustic prism are all mounted on a two-directional motion stage which is computer controlled. The two motion directions of the stage are axes X and Y depicted in Fig. 1(a). The X axis is parallel to the wave propagation direction.

The acoustic wave properties are characterized by laser interferometry [18–20] at any position on the surface. The probe beam is fixed, and the two dimensional motion stage is used for spatial scanning. A 200-nm-thick aluminum layer is deposited on the surface of the phononic crystal slab in order to obtain a uniform reflectivity whatever the position. The laser interferometer is sensitive to the vertical displacements of the surface of the slab. Heterodyning in the interferometer gives us access to amplitude and phase information. The probe beam size of the laser interferometer $10 \mu\text{m}$ is small enough to detect vertical displacements at any point in the surface of the phononic crystal slab with subwavelength resolution. The position dependent transmission spectra shown in the next sections are obtained by varying the frequency of the signal sent to the emitting transducer. The available signal frequency range is between 100 and 500 kHz, and the resolution in the frequency domain is 1 kHz.

The band structure of the phononic crystals slab was computed using a finite element method (FEM) with periodic boundary conditions [12,21]. The phononic crystal is assumed to be infinite and arranged periodically along the surface. The whole domain is split into successive unit cells, consisting of a single steel bead surrounded by the square cubic epoxy matrix. The unit cell is meshed and divided into elements connected by nodes. Bloch-Floquet periodic boundary conditions are applied at the boundaries of the unit cell. All fields are assumed to present a time-harmonic variation of the form $\exp(j\omega t)$ where ω is the angular frequency.

III. COMPLETE BAND GAP CHARACTERIZATION

The complete band gaps can in principle be identified experimentally from the transmission spectra measured along the two highest symmetry directions of the square lattice. These two directions are the ΓX and ΓM directions shown in Fig. 1(b). The acoustic wave transmission properties for both directions were first measured in an area covering one period of the phononic crystal slab, i.e., one bead. The results are presented in Fig. 2. In Fig. 1, the origin of the X axis is the rightmost edge of acoustic prism, while the origin of the Y axis is the center of the transducer. The spatial scan area extends along the X axis (Y axis, respectively) from 12 to 16 mm (-2 to 2 mm, respectively), and there are 25 points in the scan area. The transmission spectra shown are the average of the measurements at these 25 points. The measurement transmission spectra in the ΓX and ΓM directions are shown on the left-hand side of Figs. 2(a) and 2(b), respectively. Also shown is the reference transmission spec-

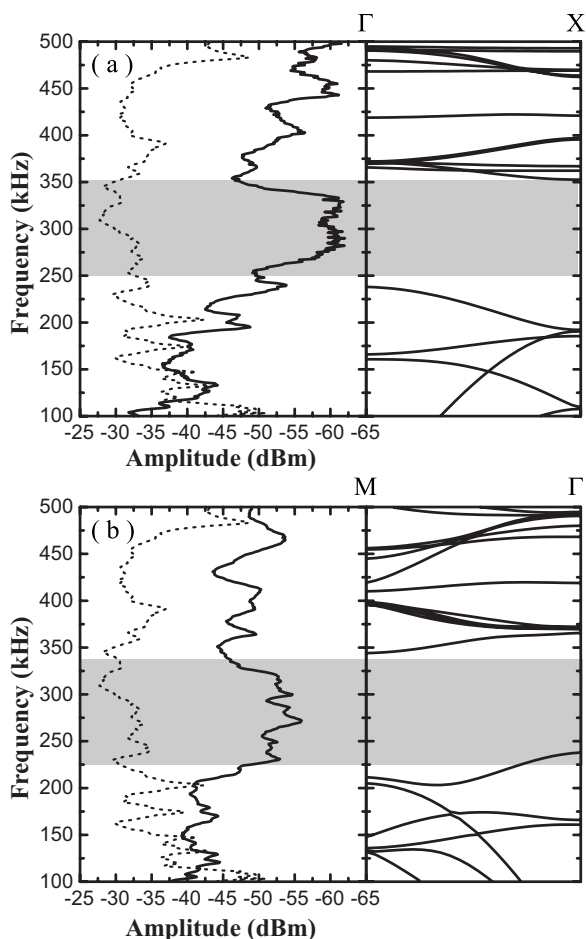


FIG. 2. Measured transmission spectrum (left-hand side) and computed band structure (right-hand side) in the (a) ΓX and (b) ΓM direction, respectively. The transmission spectra for the phononic crystal samples (solid line) and for the pure epoxy reference slab (dashed line) are compared. In the band structures, the gray areas indicate the frequency bands where attenuation caused by a band gap is apparent.

trum for a pure epoxy slab with a thickness of 4 mm. This reference spectrum is obtained with exactly the same procedure as for the phononic crystal samples. The shown data are unnormalized and displayed on a logarithmic scale. The right-hand sides of Figs. 2(a) and 2(b) display the theoretical band structures obtained using the finite element method for the ΓX and ΓM directions, respectively.

In the ΓX direction, Fig. 2(a), the gray area indicates the frequency band where attenuation is caused by a band gap. The transmission spectrum exhibits a strong attenuation from 255 to 350 kHz. Comparatively, the band gap extends from 238 to 350 kHz in the theoretical band structure. These two ranges are almost coincident. In the ΓM direction, Fig. 2(b), the experimental attenuation frequency range extends from 225 to 340 kHz, while in the theoretical band structure the band gap extends from 237 to 344 kHz. Again, there is a rather good agreement between theory and experiment. Considering the frequency range where a band gap is simultaneously apparent for both directions, the experimental complete band gap extends from 255 to 340 kHz. In the

reference transmission spectrum, there is no significant attenuation in this frequency range. The theoretical complete band gap extends from 238 to 344 kHz and thus is a little wider than the experimental one. The discrepancy can be explained by at least two arguments. The first one is the fabrication inaccuracy of the slabs, which makes the thickness of our structures not perfectly uniform. Since the band diagram depends strongly on the slab thickness, some dispersion may result. The second argument is that the elastic properties of steel and epoxy considered in the theoretical calculation may differ slightly from the actual values.

IV. ATTENUATION VERSUS DISTANCE

As already mentioned, the interferometer probe beam size is small enough to detect the spectrum at a single point on the surface of the phononic crystal slabs. This advantage can be used to investigate the variation of the attenuation with the propagation distance, as shown in Fig. 3. For this purpose, the spatial scan area is chosen as follows. In the propagation or X direction, the scan starts at the origin of the X axis, i.e., at the rightmost edge of acoustic prism, and the total scan length is 40 mm. The scan step is 1 mm. In the Y direction, as for the measurement of complete band gap, the scan area ranges from -2 to 2 mm, i.e., covers one bead, and the scan step is 1 mm again. In Fig. 3, every measurement value along the X axis is obtained as an average over the five sampling points along the Y axis. Figures 3(a) and 3(b) display the measurement results for the ΓX and ΓM oriented phononic crystal slabs, respectively. The gray maps on the left side show the variation of the amplitude on a logarithmic scale as a function of frequency (vertical axis) and propagation distance (horizontal axis). The black cycles at the bottom of each map indicate the actual position of steel beads. The white lines limit the complete band gap frequency range.

In the following discussion of the results shown in Fig. 3, it is useful to separate the frequency range in three parts: frequencies lower than, inside, and higher than the complete band gap. Figures 3(c) and 3(d) show line scans in these three regions that are extracted from Figs. 3(a) and 3(b), respectively.

For both the ΓX and the ΓM directions, the attenuation in the frequency range below the band gap is weak. In Figs. 3(c) and 3(d), the attenuation at a frequency of 150 kHz is a quite smooth function of the propagation distance in both directions and does not depend on the orientation of the lattice.

Inside the band gap, the measured displacement amplitude decays rapidly with distance. Along the ΓX and the ΓM directions, the amplitude decays most rapidly around 280 and 270 kHz, respectively. This decay is larger than 35 dB after a propagation distance of 12 mm for ΓX and 16 mm for ΓM . It is worth noticing that the distances of amplitude decay to vanishing are equal to three periods in both cases. Indeed, the period in the ΓM direction is about 17 mm, i.e., is $\sqrt{2}$ times larger than the period in the ΓX direction, which is 12 mm. Though the attenuation is dependent on the orientation of the lattice, the attenuation per period is then similar in both cases.

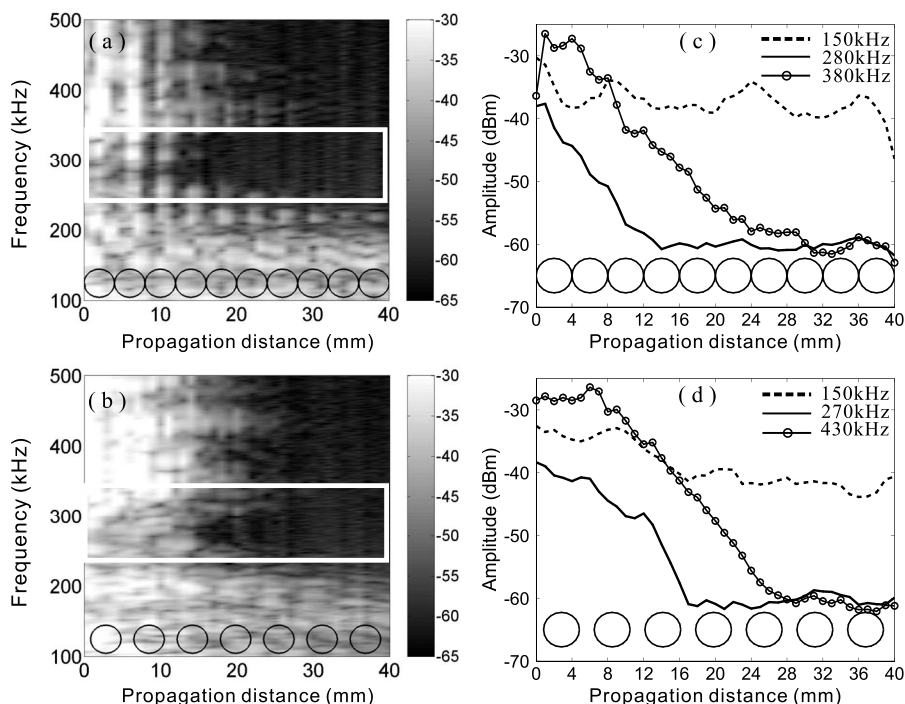


FIG. 3. Dependence of the displacement amplitude with frequency and propagation distance measured for (a) the ΓX and (b) the ΓM oriented phononic crystal slabs. The white lines in the gray maps limit the complete band gap frequency range, while the black cycles indicate the position of steel beads. The graphs (c) and (d) are extracted from the data in (a) and (b), respectively, and show line scans at three particular frequencies. The chosen frequencies lie before the complete band gap, inside it, and above it.

The variation of the attenuation with the propagation distance in the frequency range above the band gap is less expected. The two chosen representative frequencies in Fig. 3 for the ΓX and ΓM directions are 380 and 430 kHz, respectively. These frequencies are chosen such that the attenuation is minimum. For both directions, the amplitude remains approximately constant for the first two periods, then decays to the minimum detection level (-60 dBm) in 25 mm approximately.

Comparing with two-dimensional phononic crystals composed of arrays of steel cylinders in water, we remark that a decay for frequencies above the complete band gap was not particularly observed for bulk acoustic waves in the experiments of Refs. [22,23], for instance. However, this phenomenon of attenuation above the band gap was observed previously in other phononic crystals involving an epoxy matrix. It is present in the measurements of Vasseur *et al.* [15] in the case of a two-dimensional array of steel cylinders and also in the experiments of Page *et al.* [24] in the case of arrays of steel or tungsten carbide spheres. In both cases, the phononic crystals were excited with bulk waves. The natural propagation loss of epoxy is not likely to be the only origin of the attenuation above the band gap. Indeed, in the pure epoxy slab, the propagation loss of high frequency waves is not as strong as that observed in the phononic crystal slab. It may be remarked that above the band gap, almost all branches of the dispersion diagrams of Fig. 2 are rather flat, and hence represent slab modes with low group velocities. Some of them might even correspond to internal resonances of the steel spheres [25]. In any case, the wave energy becomes trapped or is restored outside of the phononic crystal with some delay. This effect combined with even moderate attenuation in epoxy could result in enhanced dissipation of energy. A numerical verification of this phenomenon would require attenuation to be included in the finite element model.

V. LINE-DEFECT WAVEGUIDE

A waveguide was formed by removing exactly one line of steel beads along the ΓX direction. The transmission spectrum of the waveguide displayed in Fig. 4 was measured starting at a distance of 24 mm, i.e., six periods away from the rightmost edge of the acoustic prism. This distance from the source is chosen so that the wave propagation inside the waveguide is stable. The measurement setup is the same as in Fig. 1. The total scan distance along the X axis is 20 mm (five periods) and the scan step is 0.4 mm. In the Y direction, the scan width is across all the waveguide width, i.e., 4 mm (one period). The scan step is 0.4 mm again. The transmis-

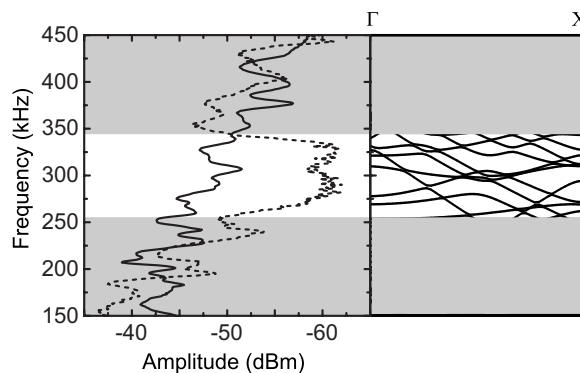


FIG. 4. Experimental transmission through a line-defect waveguide managed along the ΓX direction of the phononic crystal slab and corresponding theoretical band diagram. In the left panel, the transmission spectrum of the waveguide (solid line) is compared to the transmission spectrum of the perfect phononic crystal slab (dashed line). The right panel displays the theoretical band diagram of the waveguide. The complete band gap frequency range is located between the two gray areas.

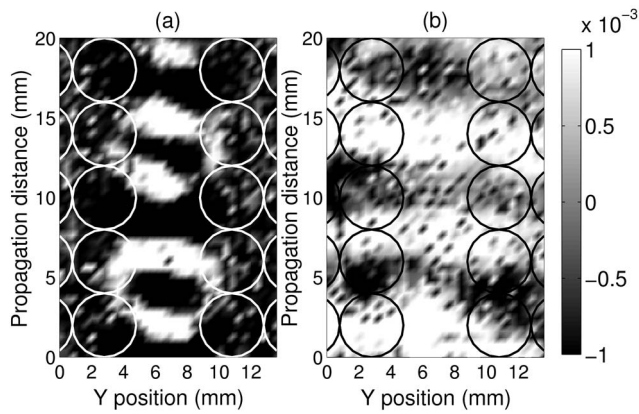


FIG. 5. Real part of the displacement amplitude of acoustic waves in the line-defect waveguide at (a) a frequency of 275 kHz (within the complete band gap) and (b) a frequency of 134 kHz (below the complete band gap). The white circles in (a) and the black circles in (b) indicate the positions of the steel beads.

sion spectrum of the waveguide shown in Fig. 4 is obtained by averaging all samples in the scan area. Figure 4 also displays the band diagram of the waveguide computed with the finite element method using a supercell technique. The meshed region includes one period in the X direction and three beads on both sides of the waveguide in the Y direction (for a total width of 28 mm). Periodic boundary conditions are applied at the facets orthogonal to the X and Y directions. As usual with the supercell technique, it is assumed that for frequencies within the complete band gap there are only evanescent waves in the Y direction, so that the simulation of guided modes propagating in the X direction is accurate. Outside the complete band gap, eigenmodes of the phononic crystal with the supercell lattice are obtained instead of eigenmodes of the waveguide. For this reason, the band structure in Fig. 4 is only displayed for frequencies within the complete band gap.

The comparison of the spectra of the waveguide and the perfect phononic crystal clearly shows that the acoustic wave transmission inside the complete band gap range is enhanced by 15 dB approximately in the waveguide case. The greatest enhancement occurs at a frequency of 275 kHz. This transmission enhancement is not uniform for all frequencies. In-

deed, the band diagram shows that propagation inside the waveguide is highly multimodal, with many defect bands appearing inside the complete band gap range. The transmission as a function of frequency then depends in a non obvious manner on the excitation of the different guided modes and their respective velocities.

The confinement of acoustic energy within the waveguide was checked by laser interferometry. Figure 5 displays the real part of the displacement amplitude measured at the surface of the phononic crystal slab. Measurements at two different frequencies are displayed. In both cases, the source is launched from the bottom of the figure. At a frequency of 134 kHz, well below the lower band gap edge, the acoustic wave is mostly propagated according to a plane wave modal shape and acoustic energy is not confined inside the waveguide. At a frequency of 275 kHz, within the complete band gap, the acoustic wave energy is seen to be highly confined laterally inside the waveguide and to propagate with a stable modal shape. This observation is an indirect confirmation of the existence of the complete band gap, since leakage would be observed if it were not present.

VI. CONCLUSION

The propagation of acoustic waves in phononic crystal slabs constituted by a square lattice array of steel beads embedded in an epoxy matrix has been studied experimentally and theoretically. A complete band gap was identified by measuring the transmission spectrum along the two most symmetric directions of the Brillouin zone by laser interferometry. The measured transmission spectra and the theoretical band structure obtained by a finite element method are in agreement and show that the complete band gap ranges from 255 kHz to 340 kHz. The dependence of the attenuation on the propagation distance was studied. Little attenuation is observed below the complete band gap and a clear exponential decay is observed within it. Unexpectedly, a pronounced unexpected decay is observed for frequencies above the complete band gap. Finally, a line-defect waveguide was formed in the ΓX direction. The transmission through the waveguide was measured and the wave field was imaged. These observations show that the waveguide efficiently confines acoustic energy within the complete band gap.

-
- [1] M. S. Kushwaha, P. Halevi, L. Dobrzynski, and B. Djafari-Rouhani, *Phys. Rev. Lett.* **71**, 2022 (1993).
 - [2] M. M. Sigalas and E. N. Economou, *Solid State Commun.* **86**, 141 (1993).
 - [3] J.-O. Vasseur, B. Djafari-Rouhani, L. Dobrzynski, M. S. Kushwaha, and P. Halevi, *J. Phys.: Condens. Matter* **6**, 8759 (1994).
 - [4] J. V. Sanchez-Perez, D. Caballero, R. Martinez-Sala, C. Rubio, J. Sanchez-Dehesa, F. Meseguer, J. Llinares, and F. Galvez, *Phys. Rev. Lett.* **80**, 5325 (1998).
 - [5] F. R. Montero de Espinosa, E. Jimenez, and M. Torres, *Phys. Rev. Lett.* **80**, 1208 (1998).
 - [6] M. M. Sigalas and N. Garcia, *J. Appl. Phys.* **87**, 3122 (2000).
 - [7] A. Khelif, B. Djafari-Rouhani, J.-O. Vasseur, P. A. Deymier, P. Lambin, and L. Dobrzynski, *Phys. Rev. B* **65**, 174308 (2002).
 - [8] M. Wilm, S. Ballandras, V. Laude, and T. Pastureau, *J. Acoust. Soc. Am.* **112**, 943 (2002).
 - [9] T. Miyashita, *Jpn. J. Appl. Phys., Part 1* **41**, 3170 (2002).
 - [10] J.-H. Sun and T.-T. Wu, *Phys. Rev. B* **74**, 174305 (2006).
 - [11] J.-C. Hsu and T.-T. Wu, *Phys. Rev. B* **74**, 144303 (2006).
 - [12] A. Khelif, B. Aoubiza, S. Mohammadi, A. Adibi, and V. Laude, *Phys. Rev. E* **74**, 046610 (2006).
 - [13] J. Gao, J.-C. Cheng, and B. Li, *Appl. Phys. Lett.* **90**, 111908 (2007).

- (2007).
- [14] J. D. Joannopoulos, R. D. Meade, and J. N. Winn, *Photonic Crystals* (Princeton University Press, Princeton, 1995).
- [15] J. O. Vasseur, P. A. Deymier, B. Chenni, B. Djafari-Rouhani, L. Dobrzynski, and D. Prevost, *Phys. Rev. Lett.* **86**, 3012 (2001).
- [16] X. Zhang, T. Jackson, E. Lafond, P. A. Deymier, and J.-O. Vasseur, *Appl. Phys. Lett.* **88**, 041911 (2006).
- [17] B. Bonello, C. Charles, and F. Ganot, *Appl. Phys. Lett.* **90**, 021909 (2007).
- [18] D. Royer and O. Casula, *Appl. Phys. Lett.* **67**, 3248 (1995).
- [19] J. V. Knuuttila, P. T. Tikka, and M. M. Salomaa, *Opt. Lett.* **25**, 613 (2000).
- [20] K. Kokkonen, S. Benchabane, A. Khelif, M. Kaivola, and V. Laude, *Appl. Phys. Lett.* **91**, 083517 (2007).
- [21] S. Benchabane, A. Khelif, J.-Y. Rauch, L. Robert, and V. Laude, *Phys. Rev. E* **73**, 065601(R) (2006).
- [22] A. Khelif, A. Choujaa, B. Djafari-Rouhani, M. Wilm, S. Balandras, and V. Laude, *Phys. Rev. B* **68**, 214301 (2003).
- [23] A. Khelif, A. Choujaa, S. Benchabane, B. Djafari-Rouhani, and V. Laude, *Appl. Phys. Lett.* **84**, 4400 (2004).
- [24] J. H. Page, S. Yang, Z. Y. Liu, M. L. Cowan, C. T. Chan, and P. Sheng, *Z. Kristallogr.* **220**, 859 (2005).
- [25] D. Brill and G. Gaunard, *J. Acoust. Soc. Am.* **81**, 1 (1987).